Fracture Toughness of Hydrogen Precharged GTA Welds of Forged Stainless Steel

J.A. Ronevich[*], B.P. Somerday[*], C. San Marchi[*], H.F. Jackson[**], and K.A. Nibur[***]

[*]Sandia National Laboratories, 7011 East Ave., Livermore CA, 94550, USA
[**]Structural Integrity Associates, Inc, 5215 Hellyer Ave., San Jose CA, 95138, USA
[***]Hy-Performance Materials Testing, LLC, 17676 Paladin Dr., Bend OR, 97701, USA

Abstract

Although austenitic stainless steels are generally considered to be compatible with hydrogen environments, these materials can exhibit pronounced hydrogen-assisted cracking susceptibility, which depends on material characteristics such as alloy composition and microstructure. The purpose of this work is to examine the fracture toughness of hydrogen precharged forged 304L/308L and 21-6-9/308L gas tungsten arc (GTA) welds in which 308L is the filler metal with emphasis on the fusion zone (FZ) and the heat-affected zone (HAZ). Significant reduction in fracture toughness was observed in the FZ of both weld materials and results were comparable with previous work using annealed base metal. Crack propagation followed weld metal δ-ferrite dendrites in the FZ which suggests lower fracture resistance in the presence of hydrogen. Higher δ-ferrite fractions in 304L/308L provided more crack nucleation sites and lower resistance to crack propagation resulting in lower fracture toughness than 21-6-9/308L GTA welds. Results from HAZ tests exhibited significant variability in crack growth resistance curves. Further analysis revealed inconsistency in terminating the precrack in the HAZ which most likely contributed to the variability. Modifications of the weld piece geometry have improved the probability of positioning the precrack in the HAZ by allowing the crack to propagate parallel to the fusion zone / base metal boundary line.

Keywords: Hydrogen Embrittlement, Welds, Fracture Toughness, Stainless Steel

Introduction:

Austenitic stainless steels are known to be resistant to hydrogen-assisted fracture and exhibit significant ductility relative to other materials in hydrogen. Retention of fracture toughness in extreme environments makes these materials desirable for use in hydrogen containing pressure vessels. Weld microstructure and composition often differ from the base material and therefore may exhibit differences in fracture properties. Gas tungsten arc (GTA) weld filler metals are selected to promote retention of small fractions of δ-ferrite in the fusion zone (FZ) to prevent solidification cracking [1, 2]. However, the consequences of ferrite in the FZ of the weld can affect hydrogen transport and contribute to greater hydrogen susceptibility. The heat-affected zones (HAZ) of austenitic stainless steel welds also contribute a potential susceptibility to hydrogen-assisted fracture. Heat generated during multiple passes results in alterations of the microstructure in the base metal adjacent to the FZ and can result in reduced fracture resistance in a hydrogen environment. Despite the understanding that HAZ is an area of susceptibility, a lack of studies have characterized the hydrogen affected fracture toughness of HAZ, possibly due to the difficulty in characterizing such a small region of the weld. Previous work by Jackson *et al.* [3] focused on determining properties of the FZ in hydrogen pre-charged welds of 304L base metal with 308L filler metal and 21Cr-6Ni-9Mn (commonly referred to as 21-6-9) base metal with 308L filler metal. The base metal used was bar stock in the annealed condition and compact tension (CT) specimens were oriented so that the notch tip was located at the base of the weld centerline. Jackson *et al.* [3] characterized hydrogen pre-charged fracture toughness by generating fracture resistance, J-R curves in the FZ. HAZ could potentially be vulnerable to hydrogen and properties of the HAZ can be affected by the higher strength forged material which necessitated fabricating GTA welds out of forged base metal for the current study.

This work presents the characterization of hydrogen-assisted fracture in GTA welds of 304L and 21-6-9 forged base metal using 308L filler metal. Samples were hydrogen precharged and fracture threshold tests were performed with targeted testing of the FZ and the HAZ. Results from three point bend FZ tests from the present study using forged material are compared to previous work [3] on annealed base metal tests in CT specimen geometry. Development of tests designed to evaluate the properties of HAZ are also discussed.

Experimental:

Forged austenitic stainless steels of two different grades (304L and 21-6-9) were examined in this study. The 304L and 21-6-9 steels were forged at 843 °C (1550 °F) through a four stage process. The as-forged yield strengths were 610 MPa for 21-6-9 and 423 MPa for 304L. The compositions of 304L, 21-6-9, and 308L filler metal are listed in Table 1. Weld rings were machined out of the forgings in a J-groove or square groove geometry and GTA welded using 308L filler metal. The welds composed of 304L base metal and 308L filler metals are designated 304L/308L and similarly the 21-6-9 base metal with 308L filler metal are designated 21-6-9/308L. Three point bend (3PB) specimens were prepared for testing according to ASTM E1820-11 [4]. In the present study, 3PB geometry was used due to material size constraint of forged rings as compared to the disk shaped CT specimen used in previous work [3]. Samples were machined to a width (W) of 9.5 mm, thickness (B) of 4.7 mm, and a starter notch of 1.8 to 3 mm using 0.1 mm (0.004 in) EDM wire. Two regions were targeted for fracture toughness

testing: FZ and HAZ. Starter notch positions were centered in the FZ for analysis of FZ properties. For tests targeting the HAZ, the starter notch was offset to a location that would allow a fatigue precrack to grow a prescribed distance into the HAZ. Specimens were side grooved to help ensure straight crack fronts and improve crack size predictions [4], and the reduced thickness B_N was 3.8 mm. Samples were oriented such that crack propagation was in the radial direction (i.e. crack growth direction is from the weld root to the final pass). Fatigue precracking was performed in air at 10 Hz and a load ratio of 0.1 to final crack lengths (a_o) of approximate 4.8 mm ($a_o/W \sim 0.5$) although crack length termination was varied to target specific distances in the HAZ. Fatigue crack growth software was used under ΔK control to a final stress intensity factor K_{max} of ~ 19.8 MPa $m^{1/2}$.

The 3PB specimens were thermally precharged at 573 K in 99.9999% hydrogen gas at a pressure of 138 MPa for a minimum of 16 days. Precharging parameters were chosen to ensure that the hydrogen concentration reached a value greater than 90% of the equilibrium hydrogen concentration at the surface [5]. Hydrogen concentration values of 140 and 220 wppm for 304L and 21-6-9, respectively, vary slightly due to compositions. Hydrogen concentrations in the fusion zone were similar to values of 304L. Hydrogen concentrations were determined by inert gas fusion at a commercial laboratory (Wah Chang, Albany, OR). Following hydrogen charging and before mechanical testing, samples were stored in a freezer (< 253 K) to prevent hydrogen egress from the steels.

Rising load fracture resistance tests were performed on hydrogen precharged 3PB specimens according to ASTM E1820-11 [4]. Samples were removed from the freezer, allowed to warm to room temperature, and tested in air at 295 K. Diffusion rates of hydrogen in austenitic steel are extremely low which allows negligible egress of hydrogen at room temperature during testing [5]. A minimum of two tests were performed for each condition (FZ and HAZ) for the 304L/308L and 21-6-9/308L welds. A servo-hydraulic frame equipped with a 4.4 kN load cell was used to load the samples monotonically through constant rising actuator displacement (0.2 mm/min). The sample rested between a fixed center pin on top and two support pins on the bottom at a spacing of 4W which are attached to a moving actuator. A one armed displacement gage was attached to the moving actuator and rested on the fixed upper pin to monitor displacement. Crack positions were continuously monitored using direct current potential difference (DCPD) signal as described in ASTM E1737-96 [6]. Constant current was supplied to leads attached at W/2 on both ends of the 3PB specimen. Potential leads were attached on opposite sides of the starter notch on the front face at a spacing of W/3, and a conditioner was used to amplify the signal 10^4 times. Tests were terminated when the voltage signal increased above background by at least 15%. Following test termination, samples were heat tinted at 623 K for 1 hr and fractured apart for examination of fracture surfaces. The precrack and final crack lengths were measured optically and DCPD data were linearly scaled to the optically measured crack lengths.

Fracture resistance J-R curves were computed for each test using J-integral calculations described in ASTM E1820-11 [4]. J versus crack growth increment, Δa, were plotted and subcritical cracking threshold toughness, J_Q, was determined as the intersection of J-R curve and a 0.2 mm offset blunting line.

Fractured samples were examined in light optical or scanning electron microscopes (SEM) for analysis of fracture surfaces features. Selected samples were sectioned and the crack plane profile was examined for location of crack front with respect to the HAZ.

Results:

Figure 1 shows two light optical images of the 304L/308L weld and are representative of both welds examined in this study. Fig. 1a image was captured of the boundary line between the FZ and the base metal (BM) at the intersection of two weld passes. Grain size in the HAZ is distinguishably larger than in the BM. The weld was built up in 6 to 7 passes with the weld root located at the bottom of the image. In general, the solidification direction is from bottom to top although dendritic structures are oriented from left to right adjacent to the boundary line. Fig. 1b shows a solidification direction change associated with overlapping weld passes in the FZ manifested by changes in dendrite orientation. The FZ consists of an austenite matrix and skeletal δ-ferrite in form of dendrites. Ferrite numbers (FN) in the FZ ranged from 5-7% and 3-4% in the 304L/308L and 21-6-9/308L welds, respectively. Lower FN were measured near the root consistent with previous work [3].

Figure 2 shows a microhardness trace of the BM, HAZ, and FZ in the 21-6-9/308L and 304L/308L weld samples. Hardness values between 304L base metal and 304L/308L FZ were comparable with a distinct drop in hardness in the HAZ. Hardness values in the 21-6-9 base metal were much higher than the 21-6-9/308L FZ and a gradual decrease in hardness was observed from base metal to the FZ.

Hydrogen noticeably reduced the fracture toughness of 304L/308L and 21-6-9/308L FZ samples as evident in the crack growth resistance (J-R) curves in Fig. 3. The fracture initiation toughness (J_Q), stress-intensity factor (K_{JQ}), and crack growth resistance ($dJ/d\Delta a$) are listed in Table 2. Fracture initiation toughness, J_Q, was determined by the intersection of the R-curve and the 0.2 mm offset blunting line. The $dJ/d\Delta a$ values were determined from the slope of the J-R curve over the first 0.5 mm immediately following deviation from the blunting line. Select J-R curves of 304L/308L and 21-6-9/308L GTA welds made from annealed base metal in a disk compact tension (CT) geometry specimen were also plotted in Fig. 3 and tabulated in Table 2 from Jackson *et al.* [3] for FZ tests for comparison. If certain conditions are met J_Q values can be qualified as size independent plane-strain fracture toughness, J_{IC}, which can be converted to a more commonly used version in the literature of K_{JIC}, through the following equation

$$K_J = \sqrt{\frac{EJ}{1-\nu^2}} \qquad (1)$$

where, E is the Young's modulus, ν is Poisson's ratio, and J is the fracture initiation toughness found from the J-R curves. In all but one sample (304L/308L 3PB FZ-7) in the current study, the conditions were not met to qualify the J_Q value as J_{IC}. However, for comparison to previous work by Jackson *et al.* [3], all J_Q values have been converted to K_{JQ} in Table 2. Higher fracture toughness was observed in 21-6-9/308L FZ compared to the 304L/308L FZ samples in hydrogen charged condition as shown in Fig. 3. The J-R curves for 21-6-9/308L in the 3PB and the CT type geometry are similar with K_{JQH} values of 215 and 207 kJ/m^2, respectively. Likewise, the K_{JQH} values for 304L/308L welds of the FZ for the 3PB and CT samples were similar at 177 and 159 kJ/m^2, respectively. Differences in the crack growth resistance, $dJ/d\Delta a$, values observed in the 21-6-9/308L welds was likely due to variations in identifying DCPD transition points. The slopes of the J vs. Δa curves appear similar near the intersection of the 0.2 mm blunting curve.

The J-R curves for the hydrogen precharged 304L/308L and 21-6-9/308L GTA welds targeting the HAZ are shown in Figs. 4a and 4b. A significant amount of scatter was observed in the J-R curves for the HAZ in both welded samples. In HAZ testing, the machined notch was translated to a location adjacent to the weld that would allow extension of the precrack into the HAZ. Fig. 5a shows an optical image of the precrack extending from the machined notch to an area anticipated to be in the HAZ. The image shown in Fig. 5a was imaged prior to placing machined side grooves along the crack plane. Preliminary tests, which represent the bulk of the results reported in Fig. 4, were side grooved prior to fatigue precracking which prevented visual inspection of the termination of the precrack with respect to the etched microstructure. Crack lengths are interpreted from compliance relationships outlined in ASTM E1820 [4]. However, even in samples that were examined prior to machining side grooves, it is difficult due to crack closure to confirm that the terminal point of the precrack is in the HAZ. Several samples were polished and etched following the fracture test to identify the location of the precrack terminal point and one example of a 21-6-9/308L HAZ specimen is shown in Fig. 5b. In Fig. 5b, it can be observed that the precrack extended into the FZ, in which crack propagation was from bottom to top. Crack propagation during the fracture toughness test was observed to follow the δ-ferrite dendrites along the solidification direction in the FZ and travel deeper into the FZ. Two factors that contribute to the difficulty in growing a precrack into the HAZ are: precision of precrack distance control, and the current J-groove design for GTA welding results in a FZ/BM interface that is not parallel to the crack front. Compliance relationships are used in the software to determine crack lengths and terminate the test at a prescribed distance which is typically accurate to 10% of the precrack. This would be sufficient in most tests where the precracking distance is not as sensitive but in the current design for HAZ samples, the GTA weld pieces are machined to have a taper of ~10°. Extension of the precrack slightly longer than anticipated results in extension of precrack into FZ as shown in Fig. 5b. Conversely, if the precrack length is terminated prematurely, the test may be sampling the unaffected BM. The implications of this weld geometry are discussed in the proceeding paragraphs.

Fig. 6a shows the fracture surface of 304L/308L FZ-7 which was precharged in hydrogen and fracture tested. The end of the precrack can be observed at the bottom of the image and the crack growth direction is from bottom to top (orientation is the same for all images). Crack growth appears to be consistent with previous results [3], in which microcracks initiate at weld ferrite and propagate along dendritic structures. Fracture surfaces of 21-6-9/308L FZ samples were similar to Fig. 6a. In non-charged condition, all samples exhibited only dimples and the absence of dendritic features. Fig. 6b shows the fracture surface of 21-6-9/308L HAZ-17. A noticeable change in surface relief can be observed at the transition point from precrack to the initiation of the fracture test (i.e. the crack plane drops deeper into the sample during the fracture test). Furthermore, dendritic structures are observed in specific locations which suggests that the crack propagated into the FZ for a portion of the fracture test. It is unclear, however, whether crack propagation initiated in the HAZ and then propagated into the FZ or whether the precrack was extended into the FZ (similar to Fig. 5b) and then the resulting test was entirely of the FZ. More microscopy needs to be invested to confirm. Fig. 6c shows the fracture surface of 304L/308L HAZ-18. The fracture surface is predominantly composed of transgranular cleavage. The fracture plane remained coincident with the precrack plane and the absence of dendritic features suggests that the crack plane was not in the FZ. However, comparison of samples selected for microscopy showed that similar fracture surfaces features in different samples did not directly

correlate to similar J-R curves in Figs. 4a and 4b. For example 304L/308L HAZ-18 and HAZ-19 exhibited similar fracture features as shown in Fig. 6c, however, the J-R curves have very different trends as shown in Fig. 4a. HAZ-19 exhibits a higher fracture toughness and crack growth resistance than HAZ-18. Likewise, 21-6-9/308L HAZ-14 and HAZ-6 were sectioned and profile images were taken similar to Fig. 5b, which revealed precracks that extended into the FZ yet J-R curves show significant variability in Fig. 4b. These observations suggest that a more consistent manner of terminating the precrack in the HAZ is necessary for reproducible test results.

In order to improved consistency of targeting the HAZ for fracture testing, a weld design modification was implemented in which a square-groove part was welded to a J-groove part as shown in Fig. 7a. This design would allow for propagation of the crack parallel to the weld in the HAZ on the square groove side of the weld joint. Due to the multi-pass nature of the GTA weld process, the fusion zone will consume part of the BM with each weld pass as shown in Fig. 7b; however, in general, the weld FZ / BM interface will be closer to parallel to the crack front. Preliminary testing is underway and supports this hypothesis.

Similarities in K_{JQH} values for FZ samples between GTA welds composed of annealed or forged base metal reflect the insensitivity of the FZ properties to the strength of the base metal. The constraint imposed by a higher strength forged material is diminished when tests were performed in the center of the FZ. However, it is expected that tests performed on the HAZ composed of annealed base metal would have exhibited different properties than GTA welds composed of forged base metal due to higher strengths and therefore constraint from the forged material. A pronounced effect of the dendritic structure on crack propagation was observed. In the FZ tests, cracks propagated preferentially at δ-ferrite resulting in elongated dendritic features on the fracture surfaces. Furthermore, in samples targeted at testing the HAZ which had precracks that extended into the FZ, the crack path was observed to reorient and align parallel to the δ-ferrite during the fracture test suggesting that ferrite exhibited lower resistance to crack propagation. Higher fracture toughness was observed in the 21-6-9/308L tests compared to the 304L/308L 3PB tests suggesting that increased δ-ferrite (in 304L/308L) results in greater quantities of crack nucleation sites and lower resistance to crack propagation [3].

Table 1 Chemical Compositions (wt%) of Base Metal and Filler Metal

	Fe	Cr	Ni	Mn	Si	C	N	P	S
304L	Bal.	19.38	10.44	1.72	0.57	0.027	0.02	0.021	0.002
21-6-9	Bal.	21.06	7.16	9.11	0.53	0.031	0.28	0.015	0.001
308L Filler	Bal.	20.5	10.3	1.56	0.50	0.028	0.055	0.006	0.012

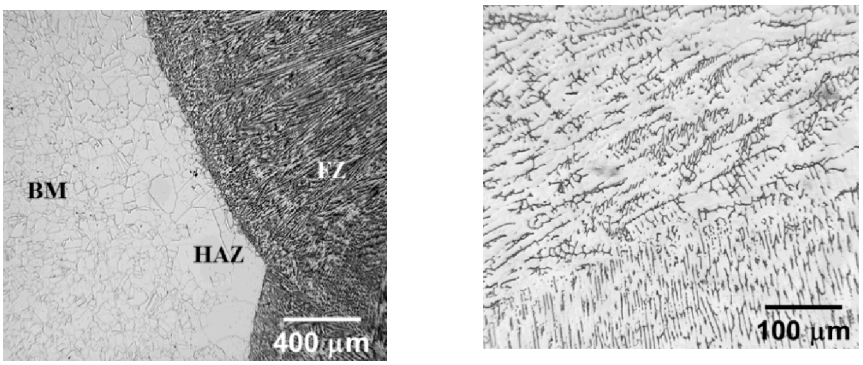

(a) (b)

Figure 1 (a) Light optical image of 304L/308L of FZ, base metal, and HAZ. (b) Higher magnification image of center of FZ with austenite matrix and skeletal δ-ferrite.

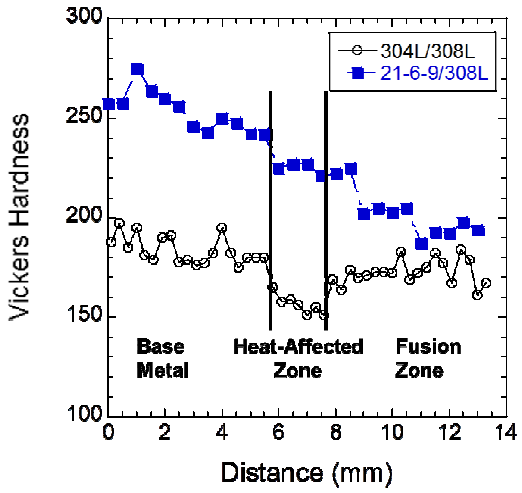

Figure 2 Vickers microhardness trace across 304L/308L and 21-6-9/308L welds using 1000 and 500 kgf force, respectively.

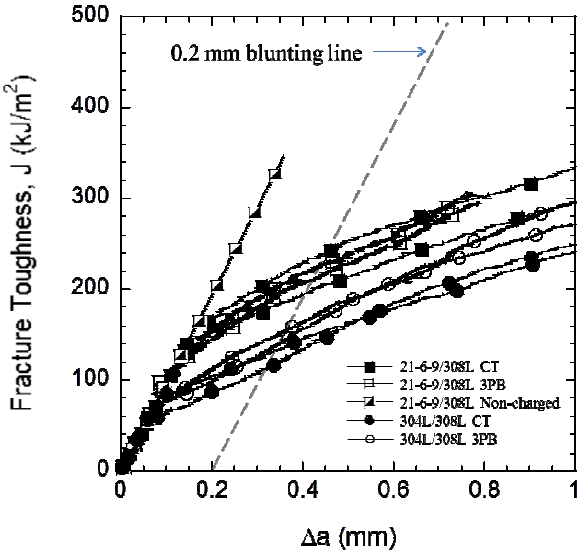

Figure 3 Crack growth resistance (J-R) curves for hydrogen precharged 21-6-9/308L and 304L/308L welds of FZ. Comparison between 3PB samples performed in the present study are compared to CT tests performed in previous work [3]. Non-charged 21-6-9/308L is plotted as representative blunting curve for both welds in non-charged condition. The dashed line represents the 0.2 mm offset blunting lines.

Table 2 Fracture initiation toughness and crack growth resistance of hydrogen precharged 304L/308L and 21-6-9/308L Welds

GTA Weld	Specimen ID	J_Q (kJ/m^2)	K_{JQ} (MPa m$^{1/2}$)	dJ/dΔa kJ/m^2/mm
304L/308L	3PB Avg.	148	177	278
	CT Avg. *(Jackson* [3])	119	159	209
21-6-9/308L	3PB Avg.	218	215	325
	CT Avg. *(Jackson* [3])	203	207	194

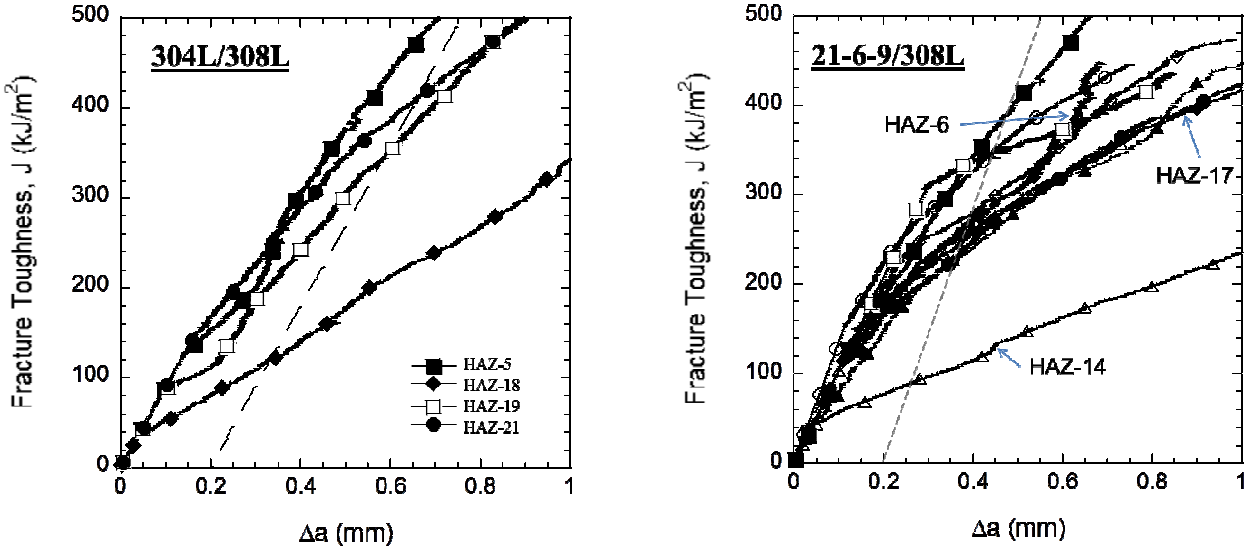

(a) (b)

Figure 4 J-R curves for (a) 304L/308L HAZ and (b) 21-6-9/308L HAZ. Selected specimens are identified in (b) for reference in further discussion. The 0.2 mm blunting lines are shown in both sets of R-curves.

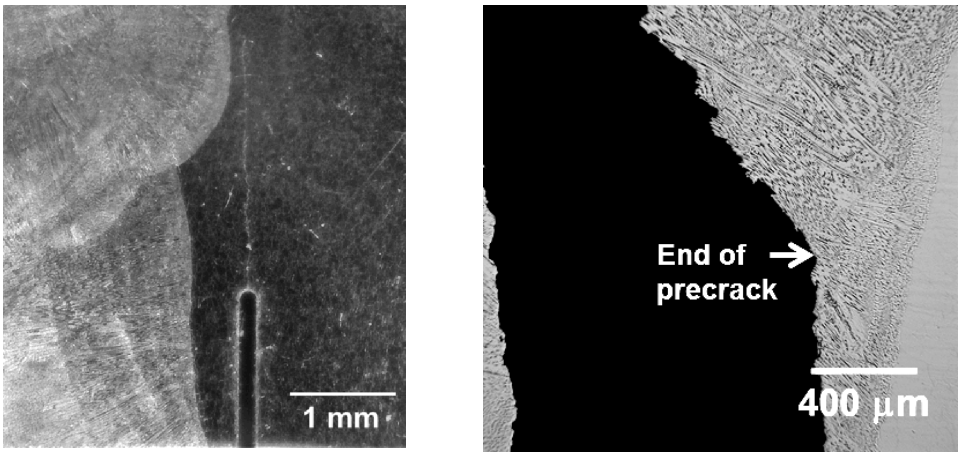

(a) (b)

Figure 5 (a) Optical image of 304L/308L HAZ 3PB sample of precrack extending out of machined notch into HAZ adjacent to a multi-pass GTA weld. (b) Extension of precrack into FZ of 21-6-9/308L HAZ-6, subsequent fracture test shows propagation of crack along δ-ferrite dendrites into the weld.

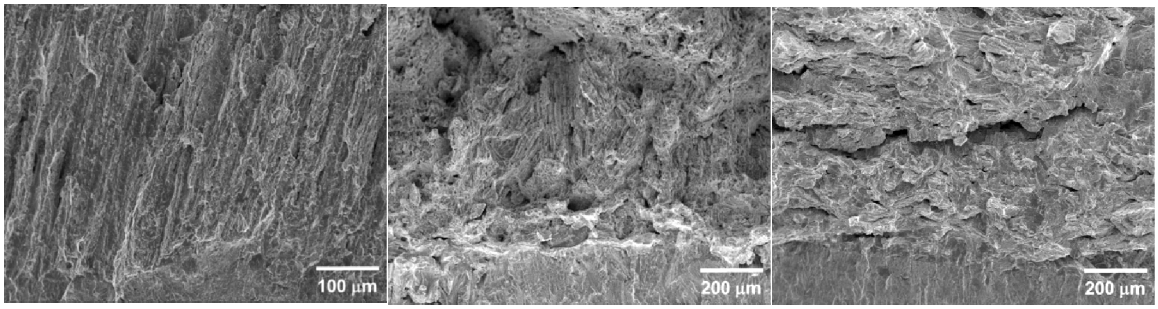

(a) (b) (c)

Figure 6 Fracture surface of hydrogen precharged 3PB of (a) 304L/308L FZ-7, (b) 21-6-9/308L HAZ-17, (c) 304L/308L HAZ-18. End of precrack can be observed in bottom of image and crack growth direction is from bottom to top.

(a) (b)

Figure 7 (a) Modified weld joint design of J-groove coupled with square-groove for GTA welding. (b) GTA weld etched to reveal FZ and BM with machined notch positioned on square-groove side of weld joint. FZ/BM interface appears to be close to parallel to notch and crack growth plane.

Conclusions:

1) Room temperature fracture toughness of 304L/308L and 21-6-9/308L welds was degraded following hydrogen precharging to levels of 140 and 220 wppm, respectively. Fracture initiation toughness (K_{JQH}) of the fusion zone (FZ) of 21-6-9/308L and 304L/308L was 215 MPa $m^{1/2}$and 177 MPa $m^{1/2}$, respectively.

2) Lower fracture toughness of 304L/308L compared to 21-6-9/308L GTA welds were attributed to higher δ-ferrite content that provide crack nucleation sites and lower resistance to crack propagation. Crack propagation was predominantly along δ-ferrite resulting in dendritic features on the fracture surface.

3) Toughness values in the current study using forged base metal were comparable to previous work on CT samples of annealed base metal, demonstrating consistency in results using different test sample geometries. Furthermore, centerline FZ properties are insensitive to strength differences in GTA welds composed of either annealed or forged base metal.

4) Inconsistency in J-R curves in HAZ samples of 21-6-9/308L and 304L/308L forged GTA welds was attributed to variability in precrack location with respect to the HAZ. Modifications of the weld piece geometry have improved the probability of positioning the precrack in the HAZ by permitting the crack to propagate parallel to the FZ/BM boundary line.

Acknowledgments:

The authors are grateful to J. Campbell for hydrogen pressure systems support, A. Gardea for metallographic preparation, and R. Nishimoto for SEM imaging. Sandia is a multi-program laboratory operated by Sandia Corporation, a wholly owned subsidiary of Lockheed Martin Corporation, for the US Department of Energy's National Nuclear Security Administration under contract DE-AC04-94AL85000.

References:

[1] J. Brooks, A. West, and A. Thompson, "Effect of weld composition and microstructure on hydrogen assisted fracture of austenitic stainless steels," *Metallurgical and Materials Transactions A,* vol. 14, pp. 75-84, 1983.

[2] J. A. Brooks and A. W. Thompson, "Microstructural development and solidification cracking susceptibility of austenitic stainless steel welds," *International Materials Reviews,* vol. 36, pp. 16-44, 1991.

[3] H. F. Jackson, K. A. Nibur, C. San Marchi, J. D. Puskar, and B. P. Somerday, "Hydrogen-assisted crack propagation in 304L/308L and 21Cr–6Ni–9Mn/308L austenitic stainless steel fusion welds," *Corrosion Science,* vol. 60, pp. 136-144, 2012.

[4] ASTM, "E1820-11 Standard Test Method for Measurement of Fracture Toughness," ed. West Conshohocken, PA, 2011.

[5] C. S. Marchi, B. P. Somerday, and S. L. Robinson, "Permeability, solubility and diffusivity of hydrogen isotopes in stainless steels at high gas pressures," *International Journal of Hydrogen Energy,* vol. 32, pp. 100-116, 2007.

[6] ASTM, "E1737-96 Standard Test Method for J-Integral Characterization of Fracture Toughness," ed. West Conshohocken, PA: ASTM International, 1996.